Synthesis and Chemical and Electrochemical Characterization of Fe−S Carbonyl Clusters. X-ray Crystal Structures of $[N(PPh_3)_2]_2[Fe_5S_2(CO)_{14}]$ and $[N(PPh_3)_2]_2[Fe_6S_6(CO)_{12}]$

Francesca Calderoni,[†] Francesco Demartin,[‡] Maria Carmela Iapalucci,[†] Franco Laschi,[§] Giuliano Longoni,*[,†] and Piero Zanello[§]

Dipartimento di Chimica Fisica ed Inorganica, viale Risorgimento 4, 40136 Bologna, Italy, Dipartimento di Chimica Strutturale e Stereochimica Inorganica, via G. Venezian 21, 20133 Milano, Italy, and Dipartimento di Chimica, Pian dei Mantellini 44, 53100 Siena, Italy

Received April 20, 1995[⊗]

A reinvestigation of the redox behavior of the $[Fe_3(\mu_3\text{-}S)(CO)_9]^{2-}$ dianion led to the isolation and characterization of the new $[Fe_5S_2(CO)_{14}]^{2-}$, as well as the known $[Fe_6S_6(CO)_{12}]^{2-}$ dianion. As a corollary, new syntheses of the $[Fe_3S(CO)_9]^{2-}$ dianion are also reported. The $[Fe_5S_2(CO)_{14}]^{2-}$ dianion has been obtained by oxidative condensation of $[Fe_3S(CO)_9]^{2-}$ induced by tropylium and Ag(I) salts or SCl_2, or more straightforwardly through the reaction of $[Fe_4(CO)_{13}]^{2-}$ with SCl_2. The $[Fe_6S_6(CO)_{12}]^{2-}$ dianion has been isolated as a byproduct of the synthesis of $[Fe_3S(CO)_9]^{2-}$ and $[Fe_5S_2(CO)_{14}]^{2-}$ or by reaction of $[Fe_4(CO)_{13}]^{2-}$ with elemental sulfur. The structures of $[N(PPh_3)_2]_2[Fe_5S_2(CO)_{14}]$ and $[N(PPh_3)_2]_2[Fe_6S_6(CO)_{12}]$ were determined by single-crystal X-ray diffraction analyses. Crystal data: for $[N(PPh_3)_2]_2[Fe_5S_2(CO)_{14}]$, monoclinic, space group $P2_1/c$ (No. 14), $a = 24.060(5)$, $b = 14.355(6)$, $c = 23.898(13)$ Å, $\beta = 90.42(3)°$, $Z = 4$; for $[N(PPh_3)_2]_2[Fe_6S_6(CO)_{12}]$, monoclinic, space group $C2/c$ (No. 15), $a = 34.424(4)$, $b = 14.081(2)$, $c = 19.674(2)$ Å, $\beta = 115.72(1)°$, $Z = 4$. The new $[Fe_5S_2(CO)_{14}]^{2-}$ dianion shows a "bow tie" arrangement of the five metal atoms. The two Fe_3 triangles sharing the central Fe atom are not coplanar and show a dihedral angle of 55.08(3)°. Each Fe_3 moiety is capped by a triply bridging sulfide ligand. The 14 carbonyl groups are all terminal; two are bonded to the unique central atom and three to each peripheral iron atom. Protonation of the $[Fe_5S_2(CO)_{14}]^{2-}$ dianion gives reversibly rise to the corresponding $[HFe_5S_2(CO)_{14}]^-$ monohydride derivative, which shows an ^{1}H-NMR signal at δ −21.7 ppm. Its further protonation results in decomposition to mixtures of $Fe_2S_2(CO)_6$ and $Fe_3S_2(CO)_9$, rather than formation of the expected H_2-$Fe_5S_2(CO)_{14}$ dihydride. Exhaustive reduction of $[Fe_5S_2(CO)_{14}]^{2-}$ with sodium diphenyl ketyl progressively leads to fragmentation into $[Fe_3S(CO)_9]^{2-}$ and $[Fe(CO)_4]^{2-}$, whereas electrochemical, as well as chemical oxidation with silver or tropylium tetrafluoroborate, in dichloromethane, generates the corresponding $[Fe_5S_2(CO)_{14}]^-$ radical anion which exhibits an ESR signal at $g = 2.067$ at 200 K. The electrochemical studies also indicated the existence of a subsequent one-electron anodic oxidation which possesses features of chemical reversibility in dichloromethane but not in acetonitrile solution. A reexamination of the electrochemical behavior of the $[Fe_3S(CO)_9]^{2-}$ dianion coupled with ESR monitoring enabled the spectroscopic characterization of the $[Fe_3S(CO)_9]^-$ radical monoanion and demonstrated its direct involvement in the generation of the $[Fe_5S_2(CO)_{14}]^{n-}$ ($n = 0, 1, 2$) system.

Introduction

The chemistry of transition metal−chalcogenide clusters has been widely explored, due to their theoretical and structural interest, as well as their involvement in several fields.[1−5] Iron−sulfur clusters play a prominent role in such a chemistry because of their potential significance as models of biological multielectron transfer agents;[6] this also stems from the suggestion of the probable existence of a third Fe-S nitrogenase which does not involve neither molybdenum nor vanadium in its composition.[6] A distinctive property of metal−sulfur clusters is their uncommon ability to undergo multiple electron-transfer steps, which do not lead to framework destruction.[7−10]

We were interested in comparing the chemical behavior of $[Fe_3(\mu_3\text{-}O)(CO)_9]^{2-}$ [11] and $[Fe_3(\mu_3\text{-}S)(CO)_9]^{2-}$,[12−15] because of their possible relationships with oxygen and sulfur atoms chemisorbed on metal surfaces. Only very few data regarding their chemical behavior are presently known and these are essentially limited to their protonation and alkylation,[11−14] or their condensation reactions to give heterometallic clusters.[16,17] The only other available information is a report on the limited redox propensity of the $[Fe_3(\mu_3\text{-}S)(CO)_9]^{2-}$ dianion; this was found to undergo a quasi-reversible one-electron anodic oxidation in dichloroethane, whose diagnostic parameters were

[†] Dipartimento di Chimica Fisica ed Inorganica.
[‡] Dipartimento di Chimica Strutturale e Stereochimica Inorganica.
[§] Dipartimento di Chimica.
[⊗] Abstract published in *Advance ACS Abstracts,* January 1, 1996.

(1) Muller, A. *Polyhedron* **1986**, *5*, 323.
(2) Dance, I; Fisher, K. *Prog. Inorg. Chem.* **1994**, *41*, 637.
(3) Lindahl, A.; Kovacs, J. A. *J. Cluster Sci.* **1990**, *1*, 29.
(4) Kanatzidis, M. G.; Huang, S.-P. *J. Coord. Chem. Rev.* **1994**, *130*, 509.
(5) Roof, L. C.; Kolis, J. W. *Chem. Rev.* **1993**, *93*, 1037.
(6) Eldredge, P. E.; Averill, B. A. *J. Cluster Sci.* **1990**, *1*, 269 and references therein.
(7) Zanello, P. *Chem. Coord. Rev.* **1988**, *83*, 199.
(8) Zanello, P. *Chem. Coord. Rev.* **1988**, *87*, 1.
(9) Zanello, P. *Struct. Bonding (Berlin)* **1992**, *79*, 101.
(10) Zanello, P. In *Stereochemistry of Organometallic and Inorganic Compounds*; Zanello, P., Ed., Elsevier: Amsterdam, 1993; Vol. 5, p 163.
(11) Ceriotti, A.; Resconi, L.; Demartin, F.; Longoni, G.; Manassero, M.; Sansoni, M. *J. Organomet. Chem.* **1983**, *249*, C35.
(12) Markò, L.; Takàcs, J.; Papp, S.; Markò-Monostory, B. *Inorg. Chim. Acta* **1980**, *45*, L189.
(13) Markò, L. *J. Organomet. Chem.* **1981**, *213*, 271.
(14) Markò, L.; Takacs, J. *Inorg. Synth.* **1989**, *26*, 243.
(15) Al-Ani, F. T.; Hughes, D. L.; Pickett, C. J. *J. Organomet. Chem.* **1986**, *307*, C31.
(16) Schauer, C. K.; Shriver, D. F. *Angew. Chem., Int. Ed. Engl.* **1987**, *26*, 255.
(17) Schauer, C. K.; Voss, E. J.; Sabat, M.; Shriver, D. F., *J. Am. Chem. Soc.* **1989**, *111*, 7662.

0020-1669/96/1335-0898$12.00/0

indicative of the relative instability of the electrogenerated $[Fe_3S(CO)_9]^-$ species.[18]

Since no attempt has been made to clarify the nature of its decomposition products, it was of interest to reinvestigate the redox behavior of $[Fe_3(\mu_3\text{-}S)(CO)_9]^{2-}$ with the aim to isolate some further example of Fe−S carbonyl clusters, and to extend these studies to the corresponding $[Fe_3(\mu_3\text{-}O)(CO)_9]^{2-}$ congener. As a result, we now report the new $[Fe_5S_2(CO)_{14}]^{2-}$, $[Fe_5S_2(CO)_{14}]^-$, and $[HFe_5S_2(CO)_{14}]^-$ clusters; as a corollary, we have spectroscopically characterized the paramagnetic $[Fe_3S(CO)_9]^-$ monoanion and found new syntheses of the known $[Fe_3(\mu_3\text{-}S)(CO)_9]^{2-}$ and $[Fe_6S_6(CO)_{12}]^{2-}$ [19] dianions. Both the $[Fe_5S_2(CO)_{14}]^{2-}$ and $[Fe_6S_6(CO)_{12}]^{2-}$ dianions have been characterized by X ray studies on their $[N(PPh_3)_2]^+$ salts.

Results and Discussion

1. Synthesis and Reactivity of the $[Fe_3S(CO)_9]^{2-}$, $[Fe_5S_2(CO)_{14}]^{2-}$, and $[Fe_6S_6(CO)_{12}]^{2-}$ Dianions. The reported syntheses of the $[Fe_3S(CO)_9]^{2-}$ dianion involve either the deprotonation of the parent $[H_{2-n}Fe_3S(CO)_9]^{n-}$ ($n = 0, 1$) hydrides, which are in turn obtained by a self-assembling reaction of $[HFe(CO)_4]^-$ and S^{2-} ions on acidification,[12] or the reduction under a carbon monoxide atmosphere of $[Fe_4S_4(SPh)_4]^{2-}$ with $LiBu^t$.[15] Although the first synthesis works well, particularly under a CO pressure,[14] a more direct approach seemed possible. Since $[Fe_3O(CO)_9]^{2-}$ has been obtained by reaction of $[Fe_3(CO)_{11}]^{2-}$ with dry air,[11] we investigated the related reaction 1 as a potentially alternate synthesis for the $[Fe_3S(CO)_9]^{2-}$

$$[Fe_3(CO)_{11}]^{2-} + {}^1/_4S_8 \rightarrow [Fe_3S(CO)_9]^{2-} + CO + COS \quad (1)$$

dianion. Initial experiments, in which elemental sulfur was used either in tetrahydrofuran (THF) or dichloromethane in the absence of activators, were unsatisfactory because exceedingly long periods of time were necessary in order to observe reaction. Better results were obtained by using the charge-transfer piperidine−sulfur adduct. The $[Fe_3S(CO)_9]^{2-}$ dianion was directly obtained in good yields (60−70% based on the $[Fe_3(CO)_{11}]^{2-}$ salt) in mixture with a red-purple byproduct showing carbonyl infrared absorptions (ν_{CO} in acetonitrile at 2040 s, 2010 s, 1965 s cm^{-1}). These were very similar but not coincident with those of the $[Fe_6S_6(CO)_{12}]^{2-}$ (ν_{CO} in acetonitrile at 2032, 2004 and 1943 cm^{-1})[19] dianion. This prompted an X-ray analysis (see next), which confirmed the above nature of the purple byproduct.

As shown in Scheme 1, which summarizes our findings in the chemistry of the Fe-S carbonyl clusters, the $[Fe_6S_6(CO)_{12}]^{2-}$ dianion and $Fe_2S_2(CO)_6$[20] progressively become the major products of reaction **1** on further addition of the sulfur-piperidine adduct, due to the consecutive reactions with sulfur of both $[Fe_3S(CO)_9]^{2-}$ and $[Fe_6S_6(CO)_{12}]^{2-}$. A similar mixture of $[Fe_6S_6(CO)_{12}]^{2-}$ and $Fe_2S_2(CO)_6$ has also been obtained by reaction in dichloromethane of $[Fe_4(CO)_{13}]^{2-}$ with the sulfur-piperidine adduct.

The observation that $[Fe_3S(CO)_9]^{2-}$ could be directly obtained from $[Fe_3(CO)_{11}]^{2-}$ prompted an investigation of other sulfur sources (e.g. C_2H_4S, CS_2, S_2Cl_2, SCl_2); the best results have been obtained on adopting SCl_2, as a result of its ready and quantitative reaction and ease of calibration. Thus, the synthesis of $[Fe_3S(CO)_9]^{2-}$ can be conveniently carried out (70% yields) by addition of SCl_2 in small portions to a stirred solution of $[Fe_3(CO)_{11}]^{2-}$ under a nitrogen atmosphere, while monitoring

Scheme 1[a]

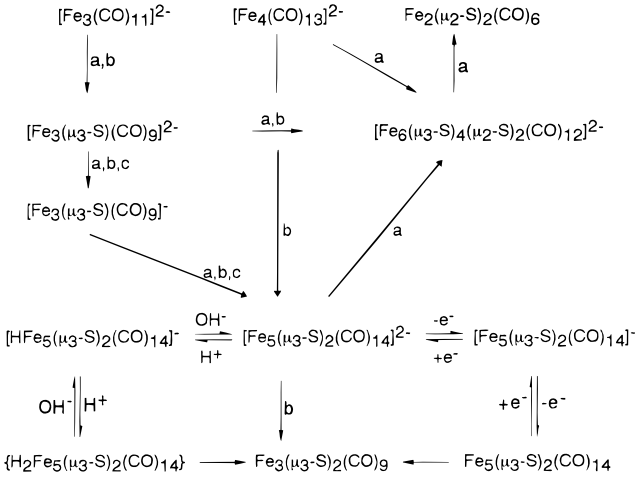

[a] (a) S_8-piperidine in THF; (b) SCl_2 in THF; (c) $AgBF_4$ in THF or tropylium tetrafluoroborate in acetonitrile.

by IR. According to the formal stoichiometry in eq 2, infrared

$$3[Fe_3(CO)_{11}]^{2-} + 2SCl_2 \rightarrow 2[Fe_3S(CO)_9]^{2-} + 2Fe(CO)_5 + Fe^{2+} + 4Cl^- \quad (2)$$

monitoring shows that $[Fe_3S(CO)_9]^{2-}$ and $Fe(CO)_5$ are formed concomitantly, and the reaction is generally complete after addition of ca. 0.7−0.8 mol of SCl_2 per mole of $[Fe_3(CO)_{11}]^{2-}$. Under these experimental conditions, the only other detectable byproducts are the $[HFe_3S(CO)_9]^-$ hydride and the previously unknown $[Fe_5S_2(CO)_{14}]^{2-}$ dianion, which are sometime obtained in trace amounts. The former probably arises from protonation of the parent dianion due to the accidental presence of moisture and the consequent hydrolysis of SCl_2; the latter derives from the subsequent oxidative condensation of $[Fe_3S(CO)_9]^{2-}$ induced by SCl_2. Both the $[Fe_5S_2(CO)_{14}]^{2-}$ and $[HFe_3S(CO)_9]^-$ impurities are readily eliminated by treatment of the THF reaction solution with sodium diphenyl ketyl, as a result of their almost quantitative reconversion to $[Fe_3S(CO)_9]^{2-}$.

The oxidation of both $[Fe_3O(CO)_9]^{2-}$ and $[Fe_3S(CO)_9]^{2-}$ has been investigated with several oxidizing agents and in different solvents, as well as electrochemically (see next section). The chemical oxidation with 1 equiv of $AgBF_4$ in THF solution at room temperature of either $[Fe_3O(CO)_9]^{2-}$ or $[Fe_3S(CO)_9]^{2-}$ initially results into a shift (*ca.* 25 cm^{-1}) of the carbonyl absorptions of both at higher wavenumbers. Concomitant ESR monitoring reveals the presence of paramagnetic species showing signals with g values of 2.052 and 2.047, respectively. The latter has been shown by coupled electrochemical and ESR studies to be due to the paramagnetic $[Fe_3S(CO)_9]^-$ monoanion. However, the intensity of the ESR signal is exceedingly low and, furthermore, the resulting baricentre of the infrared absorptions (*ca.* 1950 cm^{-1}) is barely attributable to the presence in solution purely of such a derivative (for instance, the $[HFe_3S(CO)_9]^-$ monoanion displays the baricenter of its carbonyl absorptions at ca. 1980 cm^{-1}). It appears, therefore, more likely to suggest that the above shift of the infrared absorptions is essentially due to the presence in solution of diamagnetic species probably arising from coordination of the silver ion either to the lone pair of the μ_3-capping heteroatoms, or across a Fe−Fe bond of the $[Fe_3E(CO)_9]^{2-}$ cluster, as for the related $[M\{Fe_3Se(CO)_9\}_2]^{2-}$ (M = Cd, Hg) compounds,[21] rather than the $[Fe_3E(CO)_9]^-$ (E = O, S) monoanion. Both suggested silver

(18) Honrath, U.;Vahrenkamp, H. *Z. Naturforsch., B* **1984**, *39*, 545.
(19) Lilley, G.; Sinn, E.; Averill, B. A. *Inorg. Chem.* **1986**, *25*, 1073.
(20) Wei, C. H.; Dahl, L. F. *Inorg. Chem.* **1965**, *4*, 1.
(21) Shieh, M.; Tsai, Y.-C. *Inorg. Chem.* **1994**, *33*, 2303.

adducts are unstable. However, whereas the silver adduct of $[Fe_3O(CO)_9]^{2-}$ mainly decomposes to a mixture of the starting material and the red-violet $[HFe_3(CO)_{11}]^-$, the corresponding $[Fe_3S(CO)_9]^{2-}$ silver adduct gives rise to the new green-brown $[Fe_5S_2(CO)_{14}]^{2-}$ dianion (ν_{co} in THF at 2032 w, 2009 vw, 1995 vs, 1977 s, 1964 ms, 1941 m, 1918 w) in good yields. In keeping with the above interpretation, IR monitoring of the corresponding oxidation of $[Fe_3S(CO)_9]^{2-}$ with tropylium tetrafluoroborate only discloses the progressive growth of carbonyl absorptions due to the $[Fe_5S_2(CO)_{14}]^{2-}$ dianion, even if the concomitant presence of $[Fe_3S(CO)_9]^-$ impurities is detected by ESR. The conversion of the orange-red $[Fe_3S(CO)_9]^{2-}$ into the green-brown $[Fe_5S_2(CO)_{14}]^{2-}$ dianion is generally complete upon addition of ca. 1.2 equiv of silver or tropylium tetrafluoroborate. The $Fe(CO)_4$ moiety formally missing in the above oxidative condensation is mainly eliminated as a mixture of $Fe_3(CO)_{12}$, $Fe(CO)_5$, and iron metal. The resulting salts of the $[Fe_5S_2(CO)_{14}]^{2-}$ dianion have been isolated as microcrystalline solids by filtering the reaction solutions and precipitation with toluene.

As shown in Scheme 1, the $[Fe_5S_2(CO)_{14}]^{2-}$ dianion can also be directly obtained from either $[Fe_3(CO)_{11}]^{2-}$ or $[Fe_4(CO)_{13}]^{2-}$ by reaction with SCl_2. On using $[Fe_3(CO)_{11}]^{2-}$ as starting material, the synthesis of $[Fe_5S_2(CO)_{14}]^{2-}$ requires an overall amount of ca. 1.2−1.4 equiv of SCl_2. As inferable from separate experiments on preformed samples of $[Fe_3S(CO)_9]^{2-}$, the SCl_2 in excess with respect to the stoichiometry in eq 2 induces the oxidative condensation of the latter. The major impurities present in solution at the end of the reaction are the neutral $Fe(CO)_5$, $Fe_3S_2(CO)_9$,[22] and $Fe_2S_2(CO)_6$ derivatives and the purple $[Fe_6S_6(CO)_{12}]^{2-}$ dianion, which can be separated from $[Fe_5S_2(CO)_{14}]^{2-}$ only with some difficulties due to insufficient differential solubility in organic solvents of most of their salts.

The formation of inseparable byproducts in the synthesis of $[Fe_5S_2(CO)_{14}]^{2-}$ is strongly depressed on substituting $[Fe_3(CO)_{11}]^{2-}$ with $[Fe_4(CO)_{13}]^{2-}$ salts, as starting material. In the latter case, the whole process conforms to eq 3.

$$4[Fe_4(CO)_{13}]^{2-} + 6SCl_2 \rightarrow [Fe_5S_2(CO)_{14}]^{2-} + 2Fe_3S_2(CO)_9 + 2Fe(CO)_5 + 3Fe^{2+} + 12Cl^- + 10CO \quad (3)$$

According to the formal stoichiometry of eq 3, the reaction is complete with ca. 1.4−1.5 mol of SCl_2 per mole of initial $[Fe_4(CO)_{13}]^{2-}$. Although the concomitant formation of $Fe_3S_2(CO)_9$, $Fe(CO)_5$, and Fe^{2+} salts as byproducts is detrimental for the yields, these are readily eliminated by evaporation under vacuum and washing of the residue with toluene and water. Therefore, under these experimental conditions, the resulting crude material is constituted by almost pure $[Fe_5S_2(CO)_{14}]^{2-}$ salts, which have been crystallized by layering toluene or isopropyl alcohol over their THF or acetone solutions, respectively, with 15−20% overall yields.

The $[Fe_5S_2(CO)_{14}]^{2-}$ dianion is stable in solution under an inert atmosphere and does not react with CO at atmospheric pressure. As shown in Scheme 1, it reacts with protonic acids (H_2SO_4 or H_3PO_4) to give the corresponding monohydride derivative. The green-brown $[HFe_5S_2(CO)_{14}]^-$ monoanion shows infrared carbonyl absorptions in THF at 2031 s, 2004 m, 1980 ms, and 1964 m cm^{-1} and a ^{1}H-NMR signal at δ −21.72 ppm, which is suggestive of the presence of an edge bridging hydride ligand. For sake of comparison the hydride of the related $[HFe_3S(CO)_9]^-$ monoanion has been reported at δ −23.1 ppm.[11] The $[HFe_5S_2(CO)_{14}]^-$ hydride is readily deprotonated by bases and gives rise to the typical infrared absorptions of $[Fe_5S_2(CO)_{14}]^{2-}$ also on simple dissolution in ionizing solvents such as dimethyl sulfoxide (DMSO). Addition of protonic acids to $[HFe_5S_2(CO)_{14}]^-$ in CH_2Cl_2 or THF solution, followed by evaporation and extraction in toluene, gives rise to formation of a variable mixture of the $Fe_2S_2(CO)_6$ and $Fe_3S_2(CO)_9$ compounds. In spite of some efforts, we could not obtain unambiguous spectroscopic evidence of the possible intermediate formation of an $H_2Fe_5S_2(CO)_{14}$ species corresponding to the previously reported $H_2Os_5S_2(CO)_{14}$ congener.[23]

The reduction of $[Fe_5S_2(CO)_{14}]^{2-}$ in THF with sodium diphenyl ketyl sequentially affords $[Fe_3S(CO)_9]^{2-}$ and $[Fe(CO)_4]^{2-}$ as the only carbonyl products. No evidence of the existence of a possible $[Fe_5S_2(CO)_{14}]^{3-}$ species was obtained by either IR or by ESR. In contrast, the oxidation of $[Fe_5S_2(CO)_{14}]^{2-}$ with 1 equiv of silver or tropylium tetrafluoroborate in THF or dichloromethane almost quantitatively affords the brown $[Fe_5S_2(CO)_{14}]^-$ radical anion. This shows an IR (ν_{CO} in THF at 2027 s, 2015 sh, 1985 s, and 1968 m cm^{-1}) very similar to that of $[HFe_5S_2(CO)_{14}]^-$ and a strong ESR signal at $g = 2.063$. On addition of 2 equiv or more of oxidizing agent, the ESR spectrum turns silent and, as shown by IR monitoring, a mixture of $Fe_2S_2(CO)_6$ and $Fe_3S_2(CO)_9$ is obtained.

2. Electrochemical and Coupled ESR Studies of the Redox Propensity of the $[Fe_5S_2(CO)_{14}]^{2-}$ and $[Fe_3S(CO)_9]^{2-}$ Dianions. The cyclic voltammograms exhibited by $[Fe_5S_2(CO)_{14}]^{2-}$ in dichloromethane (a) and acetonitrile (b, c) solution are shown in Figure 1. In both solvents the dianion displays a cathodic process (peak A) as well as a first oxidation step (peak B) exhibiting a directly associated response in the reverse scan. In contrast, the second oxidation process (peak C) has features of reversibility in dichloromethane, but it is clearly complicated by fast chemical reactions in acetonitrile, likely because of the well known reactivity of this solvent with electronically unsaturated species.

Controlled potential coulometric tests performed in dichloromethane solution in correspondence to the first anodic process ($E_w = 0.0$ V) consume one electron/molecule. The resulting solution shows a cyclic voltammetric profile quite complementary to that shown in Figure 1a, thus pointing out the chemical reversibility of the $[Fe_5S_2(CO)_{14}]^{2-/-}$ redox change. Subsequent exhaustive oxidation at the second anodic process ($E_w = +0.5$ V) again consumes one electron/molecule, but cyclic voltammetry on the resulting solution no longer reveals the original profile, indicating the occurrence of cluster decomposition over the long time of macroelectrolysis. As far as the reduction process is concerned, the closeness of the solvent discharge prevented any ascertainment of the number of electrons involved by controlled potential coulometry; however, judging from the peak height, we may confidently assume that it involves one electron/molecule, at least over the short times of cyclic voltammetry.

Analysis[24] of the cyclic voltammograms relevant to the $[Fe_5S_2(CO)_{14}]^{2-/-}$ oxidation in dichloromethane with scan rate varying from 0.02 to 2.00 V s^{-1} shows that (i) the i_{pc}/i_{pa} ratio is constantly equal to 1, (ii) the current function $i_{pa}/v^{-1/2}$ remains substantially constant, and (iii) the peak-to-peak separation progressively increases from 67 to 165 mV. Since under the same experimental conditions the one-electron oxidation of ferrocene ($E^{o\prime} = +0.45$ V) displays a quite similar trend in peak-

(22) Wei, C. H.; Dahl, L. F. *Inorg. Chem.* **1965**, *4*, 493.

(23) Adams, R. D.; Horvath, I. T.; Yang, L. W. *Organometallics* **1983**, *2*, 1257.

(24) Brown, E. R.; Sandifer,J. R. In *Physical Methods of Chemistry*; *Electrochemical Methods*; Rossiter, B. W., Hamilton, J. F., Eds.; Wiley: New York, 1986; Vol. 2, Chapter 4.

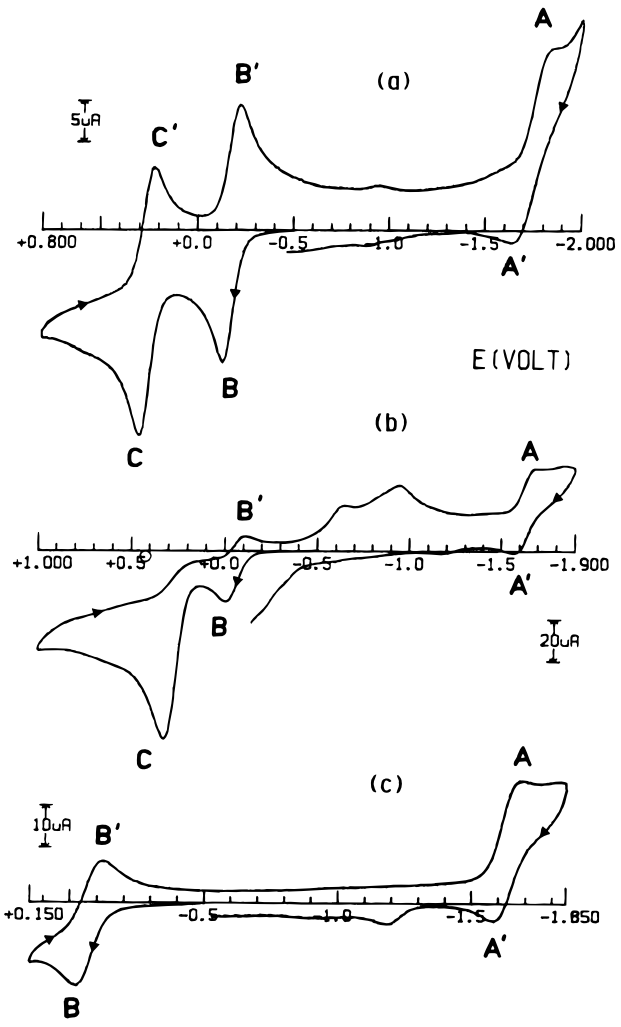

Figure 1. Cyclic voltammograms exhibited at a platinum electrode by the $[Fe_5S_2(CO)_{14}]^{2-}$ dianion under different experimental conditions: (a) CH_2Cl_2 solution containing $[NBu_4][ClO_4]$ (0.2 mol·dm^{-3}) and $[NEt_4]_2[Fe_5S_2(CO)_{14}]$ (1.68×10^{-3} mol·dm^{-3}); scan rate 0.2 V s^{-1}; (b, c) CH_3CN solution containing $[NEt_4][ClO_4]$ (0.2 mol·dm^{-3}) and $[NEt_4]_2[Fe_5S_2(CO)_{14}]$ (1.88×10^{-3} mol·dm^{-3}) at scan rates of 0.2 V s^{-1} (upper part) and 0.1 V s^{-1} (lower part), respectively.

Table 1. Redox Potentials (V vs SCE) and Peak-to-Peak Separations (mV) for the Redox Changes Exhibited by the $[Fe_5S_2(CO)_{14}]^{2-}$ Dianion

solvent	$E^{\circ\prime}{}_{0/-1}$	$\Delta E_p{}^a$	$E^{\circ\prime}{}_{-1/-2}$	$\Delta E_p{}^a$	$E^{\circ\prime}{}_{-2/-3}$	$\Delta E_p{}^a$
CH_2Cl_2	+0.26[b]	76	−0.18	84	−1.71[b]	120
CH_3CN	+0.41[c]		−0.07[b]	127	−1.53[b]	98

[a] Measured at 0.2 V s^{-1}. [b] Complicated by subsequent reactions. [c] Peak potential for irreversible processes.

to-peak separation, likely due to uncompensated solution resistances, these parameters are diagnostic of a chemically, as well as electrochemically, reversible one-electron oxidation. This suggests that upon one-electron removal the original pentairon cluster does not undergo important structural reorganizations.[10] In contrast, analysis of the cyclic voltammograms relevant to the second oxidation process $[Fe_5S_2(CO)_{14}]^{-/0}$ with scan rate clearly confirms the occurrence of chemical complications following the electron transfer. Thus, the i_{pc}/i_{pa} ratio is significantly lower than unity at low scan rates (e.g. 0.6 at 0.05 V s^{-1}) and reaches unity at higher scan rates (1.0 at 1.00 V s^{-1}). The electrode potentials for the above cited redox changes are collected in Table 1.

The X-band ESR spectral behavior of the $[Fe_5S_2(CO)_{14}]^-$ monoanion in dichloromethane solution is shown in Figure 2.

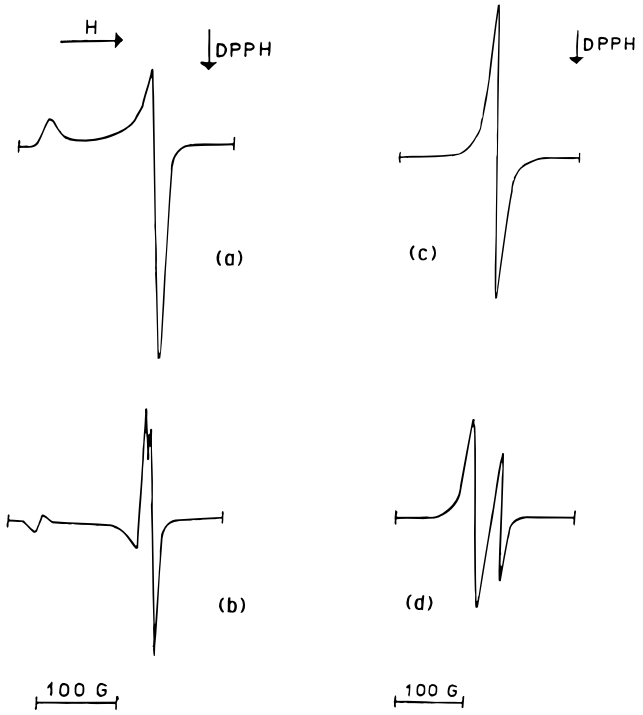

Figure 2. X-band ESR spectra of the electrogenerated $[Fe_5S_2(CO)_{14}]^-$ monoanion in CH_2Cl_2 solution: first derivative (a) and second derivative (b) spectra recorded at liquid nitrogen temperature (100 K); (c) fluid solution (T = 200 K) spectrum; (d) room temperature spectrum.

At liquid nitrogen temperature (Figure 2a,b) the line shape analysis gives evidence of a metal-centered species displaying a poorly resolved rhombic structure, the features of which are suitably interpreted in terms of a $S = {}^1/_2$ spin Hamiltonian with the unpaired electron displaying a significant orbital contribution ($g_i < g_e$).

The computer simulated ESR parameters[25] are the following: $g_l = 2.130 \pm 0.005$, $g_m = 2.042 \pm 0.005$, $g_h = 2.034 \pm 0.005$, $\langle g \rangle = {}^1/_3(g_l + g_m + g_h) = 2.069 \pm 0.005$. The line shape analysis suggests that the metal-centered unpaired electron experiences a rather unsymmetrical molecular arrangement. When the temperature is raised to the glassy-fluid transition phase ($T = 179$ K), the anisotropic features evolve to a single and unresolved peak ($g_{iso(179\ K)} = 2.067 \pm 0.005$, $\Delta H_{iso(179\ K)} = 15 \pm 5$ G). The X-band ESR spectrum of $[Fe_5S_2(CO)_{14}]^-$ recorded at $T = 200$ K is shown in Figure 2c. A further increase of the temperature causes a second high field isotropic signal to appear ($g_{iso(290\ K)} = 2.047 \pm 0.005$, $\Delta H_{iso(290\ K)} = 6 \pm 2$ G), the intensity of which reversibly increases with temperature (Figure 2d); at 290 K the molar ratio between the two signals is 2.5:1. The parameters of this additional isotropic signal are very close to those of the $[Fe_3S(CO)_9]^-$ monoanion (see next) and could indicate that $[Fe_5S_2(CO)_{14}]^-$ undergoes a reversible fragmentation equilibrium. However, the electrochemical responses of both $[Fe_5S_2(CO)_{14}]^-$ and $[Fe_3S(CO)_9]^-$ (*vide* infra) do not readily conciliate with such an interpretation. The available chemical and electrochemical data are more suggestive of an isomerization equilibrium of the former. A related equilibrium between two different deformation isomers was previously observed for $[Fe_4S_3(NO)_7]^{2-}$.[26]

The redox behavior of $[Fe_5S_2(CO)_{14}]^{2-}$ in acetonitrile solution is much more complicate. Controlled-potential coulometry in correspondence to the first oxidation process quickly consumes

(25) Lozos, G. P.; Hofman, B. M.; Franz, C. G. *QCPE* **1991**, *23*, 20.
(26) D'Addario, S.; Demartin, F.; Grossi, L.; Iapalucci, M. C.; Laschi, F.; Longoni, G.;Zanello, P. *Inorg. Chem.* **1993**, *32*, 1153.

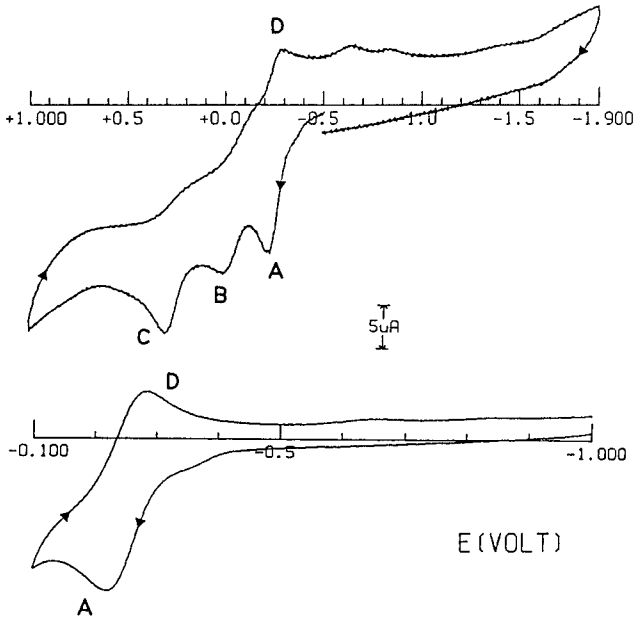

Figure 3. Cyclic voltammograms exhibited at a platinum electrode by the $[Fe_3S(CO)_9]^{2-}$ dianion in CH_3CN solution (1.1×10^{-3} mol·dm^{-3}) containing $[NEt_4][ClO_4]$ (0.2 mol·dm^{-3}) as supporting electrolyte: upper trace, scan rate 0.2 V s^{-1}; lower trace, scan rate 51.2 V s^{-1}.

one electron/molecule, but the current remains slightly higher than the background current up to an overall consumption of three electrons/molecule. Cyclic voltammetric tests after exhaustive oxidation show that only about 30% of the electrogenerated $[Fe_5S_2(CO)_{14}]^-$ monoanion is still present, thus indicating that the one-electron oxidation $[Fe_5S_2(CO)_{14}]^{2-/-}$ is accompanied by slow decomposition to further oxidizable species.

Some spectroscopic evidence reported in the previous section suggested that the chemical oxidation of $[Fe_3S(CO)_9]^{2-}$ to $[Fe_5S_2(CO)_{14}]^{2-}$ could involve the transient formation of the unstable $[Fe_3S(CO)_9]^-$ paramagnetic monoanion; indeed, an earlier report by Vahrenkamp showed that $[Fe_3S(CO)_9]^{2-}$ undergoes in dichloroethane solution a one-electron oxidation complicated by slow degradation,[18] but neither the electrogenerated $[Fe_3S(CO)_9]^-$ monoanion was spectroscopically characterized nor was the nature of the chemical complications studied. This led us to reexamine the electrochemical behavior of $[Fe_3S(CO)_9]^{2-}$. As easily deducible from Figure 3, which shows the cyclic voltammogram exhibited by $[Fe_3S(CO)_9]^{2-}$ in acetonitrile solution, the chemical complication following the one-electron oxidation is just the reorganization of the primary electrogenerated $[Fe_3S(CO)_9]^-$ to $[Fe_5S_2(CO)_{14}]^{2-}$.

As a matter of fact, the voltammetric profile exhibits a first anodic process at peak A (to which peak D is directly associated in the reverse scan), followed by the two subsequent oxidation peaks B and C, which occur at potential values just coincident with the two sequential oxidation processes exhibited by $[Fe_5S_2(CO)_{14}]^{2-}$ (see Figure 1b). Controlled-potential coulometry in correspondence to the first anodic process (peak A, $E_w = -0.2$ V) consumes one electron/molecule.

The fact that the two oxidation peaks B and C in Figure 3 arise from chemical complications following the $[Fe_3S(CO)_9]^{2-/-}$ oxidation is further supported by their almost complete disappearance at the highest scan rate of 51.2 V s^{-1} (lower trace), as well as by the fact that at low scan rate the i_{pD}/i_{pA} ratio is lower than unity and progressively increases with scan rate (some relevant values are 0.5 at 0.05 V s^{-1}, 0.7 at 0.2 V s^{-1}, and 0.9 at 1.0 V s^{-1}). The redox potentials for the oxidation process $[Fe_3S(CO)_9]^{2-/-}$ in different non-aqueous solutions are collected in Table 2. The reported i_{pD}/i_{pA} ratio, which can be assumed as an index of the relative stability of $[Fe_3S(CO)_9]^-$, indicates that the monoanion is somewhat more stable in 1,2-dichloroethane solution.

Table 2. Redox Potentials (V vs SCE) and Peak-to-Peak Separation (mV) for the Redox Changes Exhibited by the $[Fe_3S(CO)_9]^{2-}$ Dianion

solvent	$E^{\circ\prime}_{-1/-2}$	ΔE_p	i_{pD}/i_{pA}	ref
CH_3CN	−0.25	62[a]	0.6	b
CH_2Cl_2	−0.34	71[c]	0.6	b
$C_2H_4Cl_2$	−0.39	138[d]	0.9	18

[a] Measured at 0.2 V s^{-1}. [b] Present work. [c] Measured at 0.05 V s^{-1}. [d] Measured at 0.02 V s^{-1}.

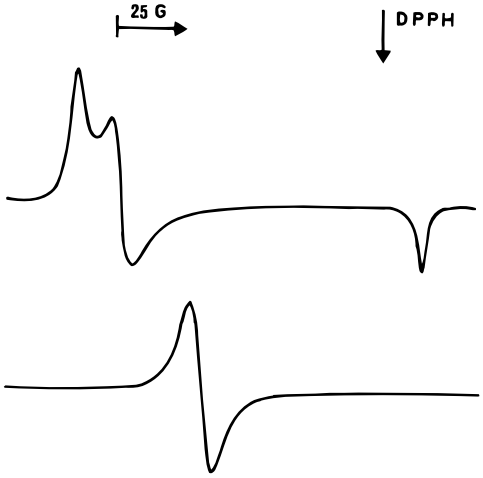

Figure 4. X-band ESR spectra of the $[Fe_3S(CO)_9]^-$ monoanion, electrogenerated in CH_2Cl_2 solution: upper trace, $T = 100$ K; lower trace, $T = 300$ K.

The X-band ESR spectrum at liquid nitrogen temperature of the $[Fe_3S(CO)_9]^-$ monoanion, which has been electrogenerated in dichloromethane at 253 K to slow down its reorganization rate, is shown in Figure 4 (upper trace). The first and second derivative analysis is consistent with the presence of a $S = {}^1/_2$ metal-in-character paramagnetic species displaying a well-resolved rhombic structure ($g_{aniso} \neq g_e$). The computed glassy parameters point out the noticeable orbital contribution of the unpaired spin density to the overall line shape and support the assumption that the unpaired electron is primarily iron-centered. The relevant parameters are as follows: $g_l = 2.079 \pm 0.002$, $g_m = 2.072 \pm 0.002$, $g_h = 1.995 \pm 0.002$, $\langle g \rangle = {}^1/_3(g_l + g_m + g_h) = 2.049 \pm 0.002$.

It can be recalled that the isostructural $[FeCo_2S(CO)_9]^-$, which has two more valence electrons, also exhibits metal-in-character paramagnetic parameters even if the unpaired electron seems mainly delocalized along the Co−Co vector.[27] Also in the present case the actual rhombic line shape suggests that the SOMO electron experiences some distortion with respect to a regular trigonal pyramidal geometry.

Above the glassy-fluid transition ($T = 180$ K) the anisotropic spectrum collapses in a single absorption as shown by the lower trace in Figure 4 ($T = 300$ K, $g_{iso} = 2.047 \pm 0.002$; $\Delta H_{iso} = 6 \pm 2$ G). The spectral behavior displays complete reversibility upon refreezing. This feature points out the relative stability of the $[Fe_3S(CO)_9]^-$ monoanion and suggests maintenance of its molecular geometry in a wide range of temperature.

3. Crystal Structures of $[N(PPh_3)_2]_2[Fe_5S_2(CO)_{14}]$ and $[N(PPh_3)_2]_2[Fe_6S_6(CO)_{12}]$. Crystals of $[N(PPh_3)_2]_2[Fe_5S_2$-

(27) Peake, B. M.; Rieger, P. H.; Robinson, B. H.; Simpson, J. *Inorg. Chem.* **1981**, *20*, 2540.

Table 3. Crystallographic Data for $[N(PPh_3)_2]_2[Fe_5S_2(CO)_{14}]$ and $[N(PPh_3)_2]_2[Fe_6S_6(CO)_{12}]$

formula	$C_{86}H_{60}Fe_5N_2O_{14}P_4S_2$	$C_{84}H_{60}Fe_6N_2O_{12}P_4S_6$
fw	1812.70	1940.78
cryst syst	monoclinic	monoclinic
space group	(No. 14) $P2_1/c$	(No.15) $C2/c$
a (Å)	24.060(5)	34.424(4)
b (Å)	14.355(6)	14.081(2)
c (Å)	23.898(13)	19.674(2)
β (deg)	90.42(3)	115.72(1)
V (Å^3)	8254(7)	8592(2)
Z	4	4
D_{calc} (g cm^{-3})	1.46	1.50
μ(Mo Kα) (cm^{-1})	10.4	12.6
min transm coeff	0.84	0.90
final R and R_w indices[a]	0.041, 0.046	0.036, 0.038

[a] $R = [\sum(F_o - K|F_c|)/\sum F_o]$. $R_w = [\sum w(F_o - K|F_c|)^2/\sum wF_o^2]^{1/2}$.

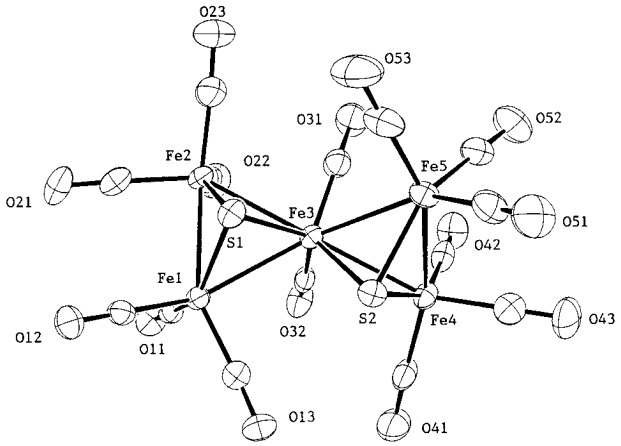

Figure 5. Perspective view of the $[Fe_5S_2(CO)_{14}]^{2-}$ dianion.

$(CO)_{14}]$ and $[N(PPh_3)_2]_2[Fe_6S_6(CO)_{12}]$ suitable for X-ray investigation were obtained by slow diffusion of toluene into their THF solutions. The crystallographic data for both compounds are collected in Table 3. An ORTEP[28] drawing of the $[Fe_5S_2(CO)_{14}]^{2-}$ anion is shown in Figure 5; selected interatomic distances and angles are reported in Table 4. The anion consists of a "bow tie" cluster of five metal atoms, arranged as two triangular groupings which share the central atom Fe(3) and contain a triply-bridging sulfide ligand. The two triangles are not coplanar, the dihedral angle between the two triangular planes being 55.08(3)°, a value close to that found in $H_2Os_5(CO)_{14}(\mu_3\text{-}S)_2$, 56.3°.[23] In the pentanuclear "bow tie" clusters, this angle usually ranges from 0 to 90°, depending on the properties of the metal and ligand atoms in the individual clusters. For instance, in the isoelectronic $Os_5(CO)_{19}$ the dihedral angle between the two Os_3 triangles is 21.2°.[29] The larger skewing observed here and in the related $H_2Os_5(CO)_{14}(\mu_3\text{-}S)_2$ depends essentially on the need of preserving (among others) a reasonable value of the S···S contact between two sulfur atoms lying on the same side of the cluster (S···S = 3.16 Å).

The idealized symmetry of the anion is C_2. The Fe(1)−Fe(2) and Fe(4)−Fe(5) bonds between the six-coordinate iron atoms are significantly shorter than the average of the Fe−Fe bonds from the central eight-coordinate Fe(3) atom to the others (average 2.560 vs 2.633 Å). This asymmetry is also reflected in the Fe−S distances, the largest bonds being those with the central Fe(3) atom.

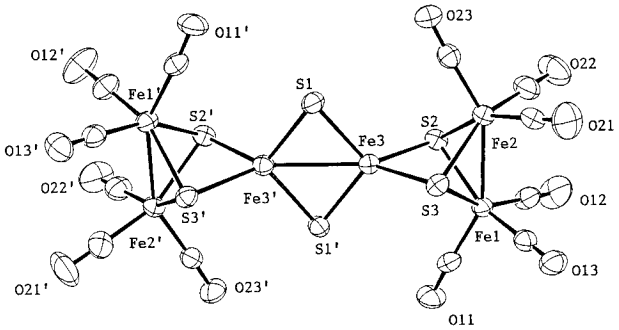

Figure 6. Perspective view of the $[Fe_6S_6(CO)_{12}]^{2-}$ dianion.

Table 4. Selected Interatomic Distances (Å) and Angles (deg) for the $[Fe_5S_2(CO)_{14}]^{2-}$ Molecular Ion

Fe−Fe		Fe−S	
Fe(1)−Fe(2)	2.556(1)	Fe(1)−S(1)	2.186(2)
Fe(1)−Fe(3)	2.628(1)	Fe(2)−S(1)	2.180(1)
Fe(2)−Fe(3)	2.634(1)	Fe(3)−S(1)	2.209(2)
Fe(3)−Fe(4)	2.626(1)	Fe(3)−S(2)	2.218(1)
Fe(3)−Fe(5)	2.643(1)	Fe(4)−S(2)	2.174(2)
Fe(4)−Fe(5)	2.564(1)	Fe(5)−S(2)	2.191(2)
Fe−C		**C−O**	
Fe(1)−C(11)	1.792(6)	C(11)−O(11)	1.144(5)
Fe(1)−C(12)	1.765(6)	C(12)−O(12)	1.151(6)
Fe(1)−C(13)	1.778(6)	C(13)−O(13)	1.144(6)
Fe(2)−C(21)	1.748(7)	C(21)−O(21)	1.163(6)
Fe(2)−C(22)	1.778(6)	C(22)−O(22)	1.150(6)
Fe(2)−C(23)	1.772(7)	C(23)−O(23)	1.148(7)
Fe(3)−C(31)	1.767(6)	C(31)−O(31)	1.173(6)
Fe(3)−C(32)	1.783(6)	C(32)−O(32)	1.165(6)
Fe(4)−C(41)	1.779(7)	C(41)−O(41)	1.144(6)
Fe(4)−C(42)	1.780(6)	C(42)−O(42)	1.143(6)
Fe(4)−C(43)	1.750(7)	C(43)−O(43)	1.164(6)
Fe(5)−C(51)	1.771(7)	C(51)−O(51)	1.140(7)
Fe(5)−C(52)	1.768(7)	C(52)−O(52)	1.154(6)
Fe(5)−C(53)	1.779(8)	C(53)−O(53)	1.155(8)
Angles (deg)			
Fe(1)−Fe(2)−Fe(3)	60.81(3)	Fe(1)−S(1)−Fe(2)	71.68(5)
Fe(1)−Fe(3)−Fe(2)	58.12(3)	Fe(1)−S(1)−Fe(3)	73.44(5)
Fe(2)−Fe(1)−Fe(3)	61.07(3)	Fe(2)−S(1)−Fe(3)	73.78(5)
Fe(3)−Fe(4)−Fe(5)	61.21(3)	Fe(3)−S(2)−Fe(4)	73.44(5)
Fe(3)−Fe(5)−Fe(4)	60.57(3)	Fe(3)−S(2)−Fe(5)	73.66(5)
Fe(4)−Fe(3)−Fe(5)	58.22(3)	Fe(4)−S(2)−Fe(5)	71.93(5)
Fe(1)−C(11)−O(11)	176.0(5)	Fe(1)−Fe(2)−S(1)	54.28(4)
Fe(1)−C(12)−O(12)	179.3(5)	Fe(1)−Fe(3)−S(1)	52.88(4)
Fe(1)−C(13)−O(13)	177.0(5)	Fe(2)−Fe(3)−S(1)	52.60(4)
Fe(2)−C(21)−O(21)	178.1(5)	Fe(2)−Fe(1)−S(1)	54.05(4)
Fe(2)−C(22)−O(22)	179.5(5)	Fe(3)−Fe(2)−S(1)	53.62(4)
Fe(2)−C(23)−O(23)	175.9(6)	Fe(3)−Fe(1)−S(1)	53.68(4)
Fe(3)−C(31)−O(31)	171.7(5)	Fe(3)−Fe(4)−S(2)	54.05(4)
Fe(3)−C(32)−O(32)	173.2(5)	Fe(3)−Fe(5)−S(2)	53.65(4)
Fe(4)−C(41)−O(41)	177.5(5)	Fe(4)−Fe(3)−S(2)	52.51(4)
Fe(4)−C(42)−O(42)	178.2(5)	Fe(4)−Fe(5)−S(2)	53.73(4)
Fe(4)−C(43)−O(43)	177.5(6)	Fe(5)−Fe(3)−S(2)	52.69(4)
Fe(5)−C(51)−O(51)	178.1(7)	Fe(5)−Fe(4)−S(2)	54.33(4)
Fe(5)−C(52)−O(52)	176.1(5)		
Fe(5)−C(53)−O(53)	177.3(6)		

The $[Fe_6S_6(CO)_{12}]^{2-}$ anion (Figure 6) has been already adequately described by Lilley et al. as a $[Fe_2S_2]^{2+}$ core coordinating two $[Fe_2S_2(CO)_6]^{2-}$ units.[19] However, due to the cation's disorder problems, the published data have an high value of the reliability index ($R = 0.099$), compared with those reported in the present paper. The anion is located on a crystallographic 2-fold axis passing through the midpoint of the

(28) Johnson, K. C. ORTEP, A FORTRAN thermal ellipsoids plot program for crystal structure illustration. Oak Ridge National Laboratory, Oak Ridge, TN, 1971.
(29) Farrar, D. H.; Johnson, B. F. G.; Lewis, J.; Raithby, P. R.; Rosales, M. J. *J. Chem. Soc. Dalton Trans.* **1982**, 2051.

Table 5. Selected Interatomic Distances (Å) and Angles (deg) for the $[Fe_6S_6(CO)_{12}]^{2-}$ Molecular Ion[a]

Fe(1)−Fe(2)	2.506(1)	Fe(3)−Fe(3)′	2.675(2)
Fe(1)−S(2)	2.308(2)	Fe(3)−S(1)	2.197(2)
Fe(1)−S(3)	2.295(2)	Fe(3)−S(1)′	2.199(2)
Fe(2)−S(2)	2.298(2)	Fe(3)−S(2)	2.310(2)
Fe(2)−S(3)	2.304(2)	Fe(3)−S(3)	2.300(2)
Fe(1)−C(11)	1.798(8)	C(11)−O(11)	1.145(7)
Fe(1)−C(12)	1.786(10)	C(12)−O(12)	1.138(9)
Fe(1)−C(13)	1.760(10)	C(13)−O(13)	1.150(9)
Fe(2)−C(21)	1.779(10)	C(21)−O(21)	1.137(9)
Fe(2)−C(22)	1.761(10)	C(22)−O(22)	1.154(9)
Fe(2)−C(23)	1.794(8)	C(23)−O(23)	1.144(7)
Fe(1)−S(2)−Fe(2)	65.92(6)	Fe(1)−Fe(2)−S(2)	57.24(6)
Fe(1)−S(2)−Fe(3)	84.89(7)	Fe(1)−Fe(2)−S(3)	56.83(6)
Fe(1)−S(3)−Fe(2)	66.03(6)	Fe(2)−Fe(1)−S(2)	56.84(6)
Fe(1)−S(3)−Fe(3)	85.41(8)	Fe(2)−Fe(1)−S(3)	57.14(6)
Fe(2)−S(2)−Fe(3)	86.43(8)	Fe(3)′−Fe(3)−S(1)′	52.47(5)
Fe(2)−S(3)−Fe(3)	86.53(8)	Fe(3)′−Fe(3)−S(2)	136.26(6)
Fe(3)−S(1)−Fe(3)′	74.98(7)	Fe(3)′−Fe(3)−S(3)	139.78(5)
		Fe(3)′−Fe(3)−S(1)	52.55(5)
Fe(1)−Fe(2)−C(21)	102.2(3)	C(11)−Fe(1)−C(12)	98.1(4)
Fe(1)−Fe(2)−C(22)	98.7(3)	C(11)−Fe(1)−C(13)	98.6(4)
Fe(1)−Fe(2)−C(23)	150.6(2)	C(12)−Fe(1)−C(13)	95.6(4)
Fe(2)−Fe(1)−C(11)	152.1(2)	C(21)−Fe(2)−C(22)	93.1(4)
Fe(2)−Fe(1)−C(12)	99.2(3)	C(21)−Fe(2)−C(23)	98.3(4)
Fe(2)−Fe(1)−C(13)	101.3(3)	C(22)−Fe(2)−C(23)	100.9(4)
S(2)−Fe(2)−C(23)	102.7(2)	S(1)−Fe(3)−S(1)′	104.96(7)
S(2)−Fe(1)−C(12)	88.2(3)	S(1)−Fe(3)−S(2)	119.30(9)
S(2)−Fe(1)−C(13)	158.1(3)	S(1)−Fe(3)−S(3)	114.04(8)
S(2)−Fe(2)−C(21)	158.8(3)	S(1)−Fe(3)−S(2)	114.94(8)
S(2)−Fe(2)−C(22)	85.7(3)	S(1)′−Fe(3)−S(3)	119.51(9)
S(2)−Fe(1)−C(11)	102.2(2)	S(2)−Fe(1)−S(3)	84.10(7)
S(3)−Fe(1)−C(11)	106.5(2)	S(2)−Fe(2)−S(3)	84.14(7)
S(3)−Fe(1)−C(12)	155.3(3)	S(2)−Fe(3)−S(3)	83.95(7)
S(3)−Fe(1)−C(13)	83.6(3)	S(3)−Fe(2)−C(22)	155.1(3)
S(3)−Fe(2)−C(23)	103.5(2)	S(3)−Fe(2)−C(21)	88.3(3)
Fe(1)−C(11)−O(11)	176.1(7)	Fe(2)−C(21)−O(21)	178.3(9)
Fe(1)−C(12)−O(12)	179.3(8)	Fe(2)−C(22)−O(22)	180.0(12)
Fe(1)−C(13)−O(13)	177.2(8)	Fe(2)−C(23)−O(23)	177.1(7)

[a] Symmetry code: ′ = $1 - x, y, {}^1/_2 - z$.

Fe(3)−Fe(3)′ bond, but its idealized symmetry is C_{2h}. Selected geometrical parameters are reported in Table 5.

Experimental Section

All reactions were carried out with standard Schlenk techniques under a nitrogen atmosphere. Solvents were dried as follows: tetrahydrofuran from sodium diphenyl ketyl, toluene from sodium sand, acetonitrile from lithium aluminum hydride. Reagent grade acetone, dichloromethane, hexane, and DMSO were deoxygenated under vacuum and stored under nitrogen. $[Fe_3(CO)_{11}]^{2-}$ and $[Fe_4(CO)_{13}]^{2-}$ salts were prepared according to literature methods.[30,31] All the other reagents were purchased from Aldrich Chemical Co. and were used without further purification.

Infrared spectra were obtained with a Perkin-Elmer 1600 interferometer using CaF_2 cells. ^{1}H-NMR spectra were recorded on a Varian Gemini spectrometer, operating at 200 MHz. ESR spectra were run on a Varian E 104 spectrometer. Apparatus and materials for electrochemical and coupled ESR measurements has been described elsewhere.[32] Potential values are referred to saturated calomel electrode SCE. Under the present experimental conditions the one-electron oxidation of ferrocene occurs at $E^{\circ\prime} = +0.38$ V in acetonitrile and at +0.45 V in dichloromethane.

1. Preparation of $[NEt_4]_2[Fe_3S(CO)_9]$ from $[NEt_4]_2[Fe_3(CO)_{11}]$. A 1.9724 g (2.68 mmol) sample of $[NEt_4]_2[Fe_3(CO)_{11}]$ was dissolved in 40 mL of dry acetonitrile. A 130 mL (2.04 mmol) aliquot of sulfur dichloride was added in small portions under stirring. The dark-red resulting solution was filtered, evaporated to dryness, dissolved in methanol and precipitated with water. This yielded 1.298 g of orange-red $[NEt_4]_2[Fe_3S(CO)_9]$ as a microcrystalline precipitate (68%). IR (ν_{co}/cm^{-1} in THF): 1999 w, 1932 s, 1905 m, 1875 w. Anal. Found (calcd): Fe, 22.85 (23.52); S, 4.41 (4.5); C, 42.53 (42.16); N, 3.73 (3.93); H, 5.87 (5.66).

The corresponding NBu_4^+, $NMe_3(CH_2Ph)^+$, and $N(PPh_3)_2^+$ salts have been similarly prepared; in those cases where significant amounts of $[HFe_3S(CO)_9]^-$ or $[Fe_5S_2(CO)_{14}]^{2-}$ were also formed, the resulting reaction solution was evaporated under vacuum, dissolved in THF and added to a concentrated THF solution of sodium diphenyl ketyl, under stirring, with monitoring of the IR spectra. The product was then isolated as described above.

2. Preparation of $[NEt_4]_2[Fe_5S_2(CO)_{14}]$ from $[NEt_4]_2[Fe_3S(CO)_9]$. A 0.144 g (0.202 mmol) sample of $[NEt_4]_2[Fe_3S(CO)_9]$ was dissolved in 15 mL of dry THF. Then 2.5 mL (0.310 mmol) of a solution of $AgBF_4$ in THF was added by syringe, under stirring. During this time the orange-red color of the solution changed to dark green. The resulting solution was filtered, evaporated to dryness, washed with water, dried under vacuum, and dissolved in THF. Crystallization from a toluene/THF solvent mixture at room temperature resulted in 0.080 g of $[NEt_4]_2[Fe_5S_2(CO)_{14}]$ as black crystals (40%). IR (ν_{co}/cm^{-1} in THF): 2034 w, 2009 vw, 1995 vs, 1977 s, 1964 ms, 1941 m, 1918 w. Anal. Found (calcd) Fe, 27.54 (28.04); S, 6.19 (6.44); C, 36.34 (36.18); N, 2.67 (2.81); H, 4.12 (4.05).

The corresponding $NMe_3(CH_2Ph)^+$ and $N(PPh_3)_2^+$ salts have been similarly prepared in acetonitrile solution, starting from the related $[Fe_3S(CO)_9]^{2-}$ salt and using tropylium tetrafluoroborate as oxidizing agent.

3. Preparation of $[NBu_4]_2[Fe_5S_2(CO)_{14}]$ from $[NBu_4]_2[Fe_4(CO)_{13}]$. A 3.00 g (2.80 mmol) sample of $[NBu_4]_2[Fe_4(CO)_{13}]$ was dissolved in 40 mL of dry THF. A 30 mL (4.7 mmol) aliquot of sulfur dichloride was added dropwise, under stirring. During this time the red color of the solution changed to brown. The resulting suspension was filtered, evaporated to dryness, washed with toluene, dissolved in methanol, and precipitated with water. The dark green precipitate was dried under vacuum and extracted with THF. A slow diffusion of toluene into the THF solution yielded 0.41 g of $[NBu_4]_2[Fe_5S_2(CO)_{14}]$ as black crystals (12%). IR (ν_{co}/cm^{-1} in THF): 2032 w, 2007 vw, 1994 vs, 1978 s, 1963 ms, 1941 m, 1916 w.

4. Preparation of $[NMe_3CH_2Ph]_2[Fe_5S_2(CO)_{14}]$ and $[NMe_3CH_2Ph]_2[Fe_6S_6(CO)_{12}]$ from $[NMe_3CH_2Ph]_2[Fe_3(CO)_{11}]$. $[NMe_3CH_2Ph]_2[Fe_3(CO)_{11}]$ (1.14 g, 1.45 mmol) was dissolved in THF (30 mL) and SCl_2 (0.2 g, 2 mmol) was added dropwise under stirring up to the disappearance of the absorption bands of the initially formed $[Fe_3S(CO)_9]^{2-}$ dianion. The resulting solution was evaporated to dryness under vacuum and the residue was washed with toluene (30 mL) in portions. The insoluble brown material was extracted in dichloromethane (30 mL) and precipitated by layering of hexane (50 mL) to obtain 0.58 g of $[NMe_3CH_2Ph]_2$ $[Fe_5S_2(CO)_{14}]$. The residue of the extraction in dichloromethane was extracted in THF to give a purple solution from which 0.21 g of $[NMe_3CH_2Ph]_2[Fe_6S_6(CO)_{12}]$ was isolated by precipitation with toluene (ν_{co}/cm^{-1} in THF at 2042 s, 2012 s and 1967 s). The corresponding $[N(PPh_3)_2]_2[Fe_6S_6(CO)_{12}]$ salt was obtained from $[NMe_3CH_2Ph]_2[Fe_6S_6(CO)_{12}]$ by metathesis in DMSO and water with $[N(PPh_3)_2]Cl$ and crystallized from acetone and isopropyl alcohol.

5. Preparation of $[NMe_3CH_2Ph][HFe_5S_2(CO)_{14}]$. $[NMe_3CH_2Ph]_2$-$[Fe_5S_2(CO)_{14}]$ (0.37 g) was dissolved in THF (10 mL) and a solution of H_2SO_4 in THF (0.1 mL in 5 mL) was added dropwise under stirring up to the disappearance of the infrared absorptions of the starting dianion. The resulting solution was evaporated to dryness under vacuum and the residue was washed with toluene (30 mL) in portions and water (30 mL). The insoluble brown material was extracted in THF (10 mL) and precipitated by layering of hexane (30 mL) to obtain 0.18 g of $[NMe_3CH_2Ph]$ $[HFe_5S_2(CO)_{14}]$ (ν_{co}/cm^{-1} in THF at 2031 s, 2004 m, 1980 ms, and 1964 m).

6. X-ray Data Collection and Structure Determination. Relevant crystallographic data are summarized in Table 3. The diffraction

(30) Kwei Lo, F. Y.; Dahl, L. F.; Longoni, G.; Chini, P. *J. Am. Chem. Soc.* **1980**, *102*, 7691.
(31) Whitmire, K. H.; Ross, J.; Cooper III, C. B.; Shriver, D. F. *Inorg. Synth.* **1982**, *21*, 66.
(32) Bianchini, C.; Laschi, F.; Masi, D.; Ottaviani, F. M.; Pastor, A.; Peruzzini, M.; Zanello, P.; Zanobini, F. *J. Am. Chem. Soc.* **1993**, *115*, 2723.

measurements were carried out on an Enraf-Nonius CAD4 diffractometer at room temperature, using graphite-monochromatized Mo Kα radiation ($\lambda = 0.710\ 73$ Å). The diffracted intensities were corrected for Lorentz, polarization, and absorption (empirical correction[33]) but not for extinction. Scattering factors for all the atomic species and anomalous dispersions corrections for scattering factors of non-hydrogen atoms were taken from ref 34. Both structures were solved by direct methods (SIR88)[35] and refined by full-matrix least-squares methods, minimizing the function $\sum w(|F_o| - k|F_c|)^2$. An anisotropic thermal parameter was assigned to all the non-hydrogen atoms, whereas the hydrogen atoms were introduced in the structure model at calculated positions (C−H 0.95 Å). Details of the crystal structure determinations are reported in the Supporting Information. All calculations were performed on a HP Vectra 486/33 computer using the Personal SDP Structure Determination Package.[36]

Acknowledgment. We thank the MURST and the EEC for financial help.

Supporting Information Available: Tables of full details of the two data collection (Tables S1 and S6), atomic coordinates of all atoms (Tables S2 and S7), anisotropic and isotropic thermal parameters of all non-hydrogen atoms (Tables S3 and S8) and distances and angles for $[N(PPh_3)]_2[Fe_5S_2(CO)_{14}]$ (Table S4) and $[N(PPh_3)_2][Fe_6S_6(CO)_{12}]$ (Table S9) (19 pages). Ordering information is given on any current masthead page.

IC950482T

(33) North, A. C.; Phillips, D. C.; Mathews, F. S. *Acta Crystallogr.* **1968**, *A24*, 351.
(34) *International Tables for X-ray Crystallography*; The Kynoch Press: Birmingham, U.K., 1974; Vol. IV.
(35) Burla, M. C.; Cascarano, G.; Fares, E.; Giacovazzo, C.; Polidori, G.; Spagna, R. *Acta Crystallogr.* **1989**, *A45*, 781.
(36) Frenz, B. A. *Comput.* in *Phys.* **1988**, *2* (3), 42. Frenz, B. A. *Crystallographic Computing 5*; Oxford University Press: Oxford, U.K., **1991**, *11*, 126.